Thin Solid Films 691 (2019) 137603

Contents lists available at ScienceDirect

Thin Solid Films

journal homepage: www.elsevier.com/locate/tsf

Growth of NbO_2 thin films on GaN(0001) by molecular beam epitaxy

Agham Posadas[a,*], Alexander Kvit[b], Alexander A. Demkov[a]

[a] Department of Physics, University of Texas at Austin, 1 University Station C1600, Austin, TX 78712, United States
[b] Department of Materials Science and Engineering, University of Wisconsin – Madison, 1509 University Avenue, Madison, WI 53706, United States

ARTICLE INFO

Keywords:
Niobium
Gallium nitride
Molecular beam epitaxy
X-ray photoelectron spectroscopy
Scanning transmission electron microscopy
Interfacial reaction

ABSTRACT

We report on the growth of epitaxial NbO_2 thin films by molecular beam epitaxy on GaN (0001). The combination of these two materials is of interest in resistive switching devices that can operate at high temperature. We show that direct deposition of Nb metal on GaN under an oxygen environment results in a substantial interfacial reaction layer. We perform detailed spectroscopic and structural analyses of the film and interface and describe their implications for the growth of this materials system.

1. Introduction

Transition metal oxide-semiconductor heterostructures are of great interest due to their potential for combining the rich electronic functionality of transition metal oxides with the wide use of semiconductors in logic, memory, and optoelectronic devices [1–3]. A number of transition metal oxides exhibit a metal–insulator transition (MIT) that can be useful for a wide variety of applications including electronic and optoelectronic switches, memristors, and tunnel field effect transistors (FETs) [4–6]. For applications in the MIT in electronics, the process for externally modulating the phase transition needs to be highly controllable. Niobium dioxide, NbO_2, is a MIT material, whose phase transition temperature is very high (800 °C) [7]. This makes it suitable for use in high temperature and high power electronic devices, where variations in the ambient temperature will not affect the state of the device. For such high temperature applications, Si is not suitable and thus there is a strong drive to use wide band gap semiconductors, such as GaN and SiC [8,9]. GaN is currently used in optoelectronic devices and blue LEDs [10,11], but it is also a semiconductor of choice for high temperature, high frequency, and high power applications because of its wide 3.4 eV direct band gap, high thermal and chemical stability and large thermal conductivity [12–14]. A possible application of NbO_2 on GaN is in fabricating hyper-FETs, which inserts a MIT material in the source terminal of a FET as a means to obtain steep switching and high on/off ratio [15]. This new FET design is being explored for reduced power consumption in conventional logic (abrupt switching) as well as for enabling new computational paradigms such as neuromorphic computing [16]. GaN-based hyper-FETs based on NbO_2 will be capable of operating at elevated temperatures. In addition, GaN is a polar material with piezoelectric properties that could be utilized for electromechanical devices and thermal sensors [17]. One possible way of inducing the MIT in NbO_2, where the MIT occurs due to a Peierls transition [18], is to alter the lattice constant using strain. By growing NbO_2 on a piezoelectric semiconductor such as GaN, one can then use an external electric field to modulate strain in the material. The combination of NbO_2 and GaN would also be potentially useful in resistive switching devices at elevated temperatures.

However, the formation of an abrupt low-defect density interface between a crystalline transition metal oxide layer and a semiconductor material remains a challenging technical problem. There are several reports of epitaxial interfaces between a functional transition metal oxide and GaN, including (Ba,Sr)TiO_3 [19,20], $YMnO_3$ [21,22], and $LiNbO_3$ [23,24]. Other groups grow rocksalt oxides such as CaO and MgO [25,26] or rutile TiO_2 [27,28], which can then be used as buffers for growing other oxides on GaN [29]. In this work, we report on the results of growing NbO_2 by molecular beam epitaxy (MBE) on GaN using a simple direct deposition process involving no surface conditioning other than degreasing and annealing of the substrate. We show that for materials system, such a direct deposition process using a metal precursor results in a reaction between the incoming Nb and O_2 flux and the GaN surface. We perform detailed chemical spectroscopic and structural analyses of the film and interface using reflection high energy electron diffraction (RHEED), x-ray photoelectron spectroscopy (XPS), in-plane X-ray diffraction (XRD), and cross-section scanning transmission electron microscopy (STEM) to better understand the resulting structure and propose a method for avoiding this interfacial reaction between NbO_2 and GaN.

* Corresponding author.
E-mail address: agham.posadas@utexas.edu (A. Posadas).

https://doi.org/10.1016/j.tsf.2019.137603
Received 15 February 2019; Received in revised form 23 September 2019; Accepted 30 September 2019
Available online 14 October 2019

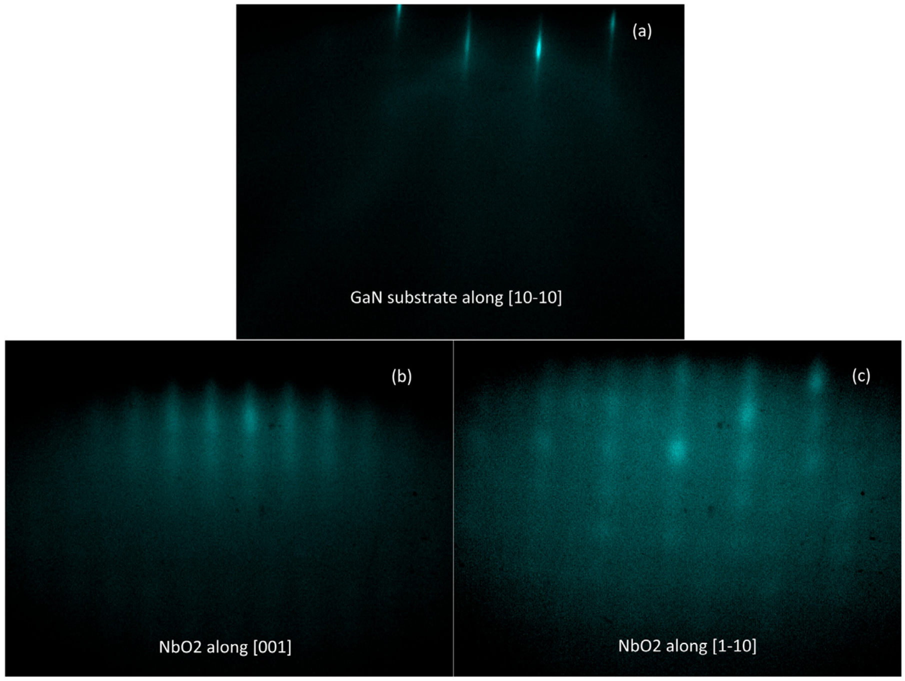

Fig. 1. RHEED images of GaN substrate and NbO_2 film. (a) RHEED image of the substrate taken along the $[10\bar{1}0]$ azimuth showing relatively flat surface with no reconstruction. (b) RHEED pattern for NbO_2 along the [001] azimuth, which is parallel to the GaN $[11\bar{2}0]$ azimuth. (c) RHEED pattern for NbO_2 along the $[1\bar{1}0]$ azimuth, which is parallel to the GaN $[10\bar{1}0]$ azimuth.

2. Experimental details

For this work, a commercially available substrate purchased from MTI Corporation was used, consisting of 0.5 µm-thick GaN (0001) on a 0.1 µm AlN (0001) buffer layer grown on single crystal Si (111). The substrate was cut into 10 mm × 10 mm pieces and degreased by sonicating for 5 min each in acetone, isopropanol, and deionized water. After degreasing, the substrate was loaded into the load lock chamber where it was first lightly outgassed in vacuum at 150 °C for 30 min prior to transferring into the growth chamber. To clean the GaN surface, the substrate was first exposed to an atomic nitrogen plasma source at a substrate temperature of 300 °C for 30 min. The radio frequency plasma source was operated using 250 W forward power under a background N_2 gas pressure of 1.3×10^{-3} Pa. After the nitrogen plasma treatment, the substrate is then annealed in vacuum at 700 °C for another 30 min. Fig. 1(a) shows the reflection high energy electron diffraction (RHEED) pattern of the cleaned GaN surface just prior to growth taken along the $[10\bar{1}0]$ azimuth showing a 1 × 1 pattern with intense diffraction spots along a circular arc, consistent with a clean, flat surface. XPS analysis of the cleaned GaN surface (not shown) shows no detectable carbon and less than 0.2 monolayer of oxygen on the surface.

For the NbO_2 film growth, we used electron beam evaporation of Nb metal in the presence of molecular oxygen in a customized DCA Instruments M600 oxide MBE reactor. The growth conditions that we previously found to yield stoichiometric NbO_2 growth on $(La,Sr)_2(Al,Ta)_2O_6$ substrates were used to grow the film on GaN [30]. The growth conditions were Nb metal flux of 2 Å/min with an oxygen pressure of 8×10^{-4} Pa at a substrate temperature of 800 °C. The Nb metal flux is first calibrated under vacuum using an INFICON quartz crystal microbalance placed near the substrate position. We use an electron energy of 7.75 keV and an emission current of 200 mA for the Nb evaporation from the electron beam source. With the Nb shutter closed, the substrate was then heated to the growth temperature at a rate of 30 °C/min after which oxygen was let into the chamber until the target pressure is reached, which took about 5 min. The Nb source shutter and main shutter are then simultaneously opened. The sample was grown for 1 hour (target thickness of 25 nm) with sample rotation. The sample surface was constantly monitored using RHEED during the growth. Fig. 1(b) and (c) shows the RHEED patterns from the surface of the sample just after growth is finished. After growth, the sample was cooled down at 40 °C/min to 200 °C under the same oxygen pressure used for the growth. After that oxygen flow was stopped and the sample transferred in situ to the XPS analysis chamber. XPS was performed using a monochromatic Al Kα source and a VG Scienta R3000 electron energy analyzer. The spectrometer is calibrated such that the measured binding energy of a clean copper sample is 932.68 eV. After XPS analysis, the samples were characterized by both out-of-plane and in-plane x-ray diffraction using Cu Kα radiation in a Rigaku Ultima IV diffractometer with an in-plane arm and thin film stage. Cross-section (S)TEM samples were prepared by mechanical wedge polishing with diamond lapping films in the $[11\bar{2}0]$ cross-section projection for GaN substrate. The samples were than ion milled in a Fischione 1050 at 5° ion mill angle. TEM conventional and high-resolution images were taken at 300 kV on FEI TF30 field emission microscope. Scanning transmission electron microscopy experiments were performed on a FEI Titan microscope with a CEOS probe aberration-corrector operated at 200 kV. STEM images were collected with a 24.5 mrad probe semi-angle, 28 pA probe current with STEM resolution of 0.8 Å. High angle annular dark field (HAADF) images were acquired in the angle range from 54 to 270 mrad. STEM electron energy loss spectroscopy (EELS) spectrum images were acquired using a 24.5 mrad probe semi-angle, spectrometer collection angle of 82 mrad, 470 pA probe current, and STEM resolution of 2.1 Å.

3. Results and discussion

3.1. Film composition

The 25 nm-thick NbO_x film grown on GaN was measured using in situ XPS immediately after growth. Fig. 2 shows XPS data from the sample for the Nb 3d, O 1s and valence band energy regions, as well as a wide range survey scan. The survey scan (Fig. 3a) confirms that only peaks arising from Nb and O are visible. The Nb 3d spectrum (Fig. 3b) shows an asymmetric spin–orbit pair of peaks whose peak maximum is

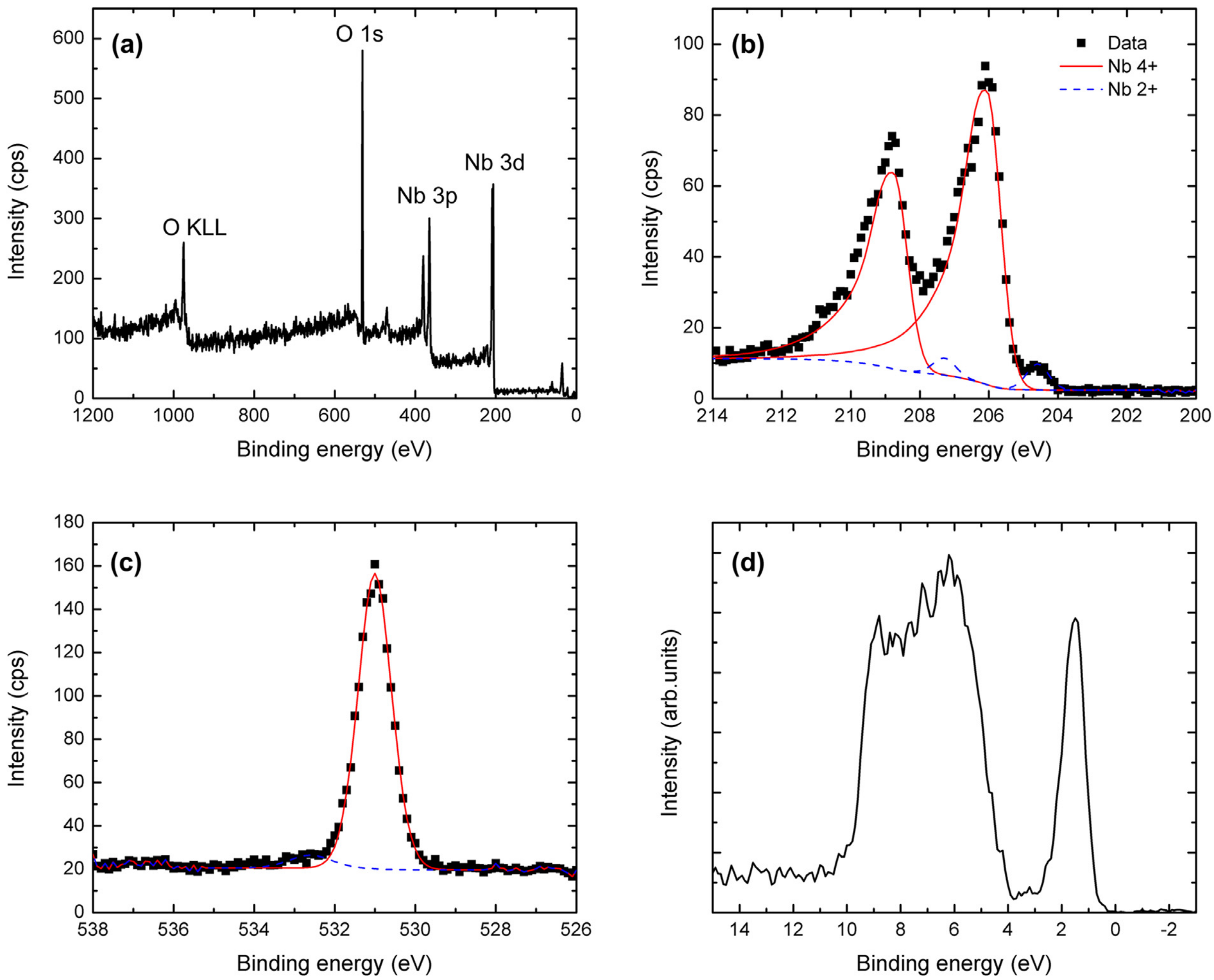

Fig. 2. XPS spectra of NbO_2 grown on GaN. (a) Survey spectrum showing peaks only from Nb and O. (b) Nb 3d spectrum showing asymmetric spin-orbit pair of peaks at a binding energy of 206.1 eV, consistent with Nb^{4+}. A minor component of Nb^{2+} at 204.6 eV can also be seen. (c) O 1s spectrum showing main peak with binding energy of 531.0 eV. A small shoulder at higher binding energy is also visible. (d) Valence band spectrum showing strong and sharp Nb 4d feature centered at around 1.5 eV binding energy and broad O 2p band centered around 7.2 eV.

at 206.0 eV. The spectrum can be fit using a Lorentzian peak with an exponential tail to high binding energy. The asymmetric nature of the peaks and its position is consistent with single phase NbO_2 [31]. There is a very small component at the lower binding energy side of the main peak (~204.6 eV) that is an indication of slight underoxidation of the sample [31]. The O 1s spectrum (Fig. 3c) shows a primary peak with a binding energy of 531.0 eV from the bulk of the film and a much smaller surface peak at 532.5 eV. The calculated O/Nb ratio using Wagner relative sensitivity factors [32] (with the number for Nb modified to give the correct stoichiometry for an Nb_2O_5 film) and accounting for sampling depth yields a value of 1.9. Fig. 3d shows the valence band spectrum of the sample where two distinct features are clearly observable: a broad peak centered around 7.2 eV (corresponding to the oxygen 2p-derived band) and a narrow peak centered at 1.5 eV (corresponding to the split-off $4d_{xy}$ Nb state of NbO_2). The shape and relative heights (~0.8) of these two features are consistent with single phase NbO_2 [31].

3.2. Film structure and epitaxy

As observed with RHEED and in-plane XRD, the in-plane orientation of the final NbO_2 film and the GaN substrate are aligned in a specific way. Fig. 1(b) and (c) shows RHEED patterns for the NbO_2 film after growth taken along the GaN $< 11\bar{2}0 >$ and $< 10\bar{1}0 >$ directions, respectively. The average RHEED spacing along the GaN $< 11\bar{2}0 >$ azimuth is determined to be about 2.9 Å and is consistent with one-half of the *c* lattice of the low-temperature body-centered tetragonal phase of NbO_2 (space group $I4_1/a$) [18]. Rotating the sample reveals that this spacing repeats every 60°, showing that the NbO_2 film has overall a pseudo-six-fold in-plane symmetry. Because the NbO_2 film has two-fold symmetry in this orientation, the RHEED data indicates that there are three symmetry-related in-plane crystalline domains present in the film. The pseudo-six-fold symmetry is also observed along the GaN $< 10\bar{1}0 >$ azimuth with the sample rotation.

XRD measurements were taken on the sample with both symmetric $2\theta-\omega$ out-of-plane scans, and grazing incidence in-plane $2\theta_\chi-\phi$ scans along the two major in-plane high symmetry directions of GaN. The XRD measurements are taken using parallel beam geometry with a beam height of 0.5 mm for out-of-plane scans and 0.1 mm for in-plane scans. Fig. 3 shows the out-of-plane XRD scan. In addition to features related to the substrate (GaN and AlN), a peak is found at 2θ ~37.5° (*d* ~ 2.4 Å) and a second much weaker peak at ~26.1° (*d* ~ 3.4 Å). The predominant film peak at 37.5° is consistent with the 440 reflection of NbO_2. This is the same out-of-plane orientation that is obtained when growing NbO_2 on $SrTiO_3$ (111) [30]. Such an orientation is also consistent with the RHEED patterns in Fig. 2. The minor peak at 26.1° may correspond to some grains of NbO_2 having 100 out of plane orientation or it may arise from the disordered polycrystalline interfacial reaction layer discussed below. A rocking curve taken about the film 440 peak has a full-width at half-maximum of 0.66°. Fig. 4(a) and (b) shows

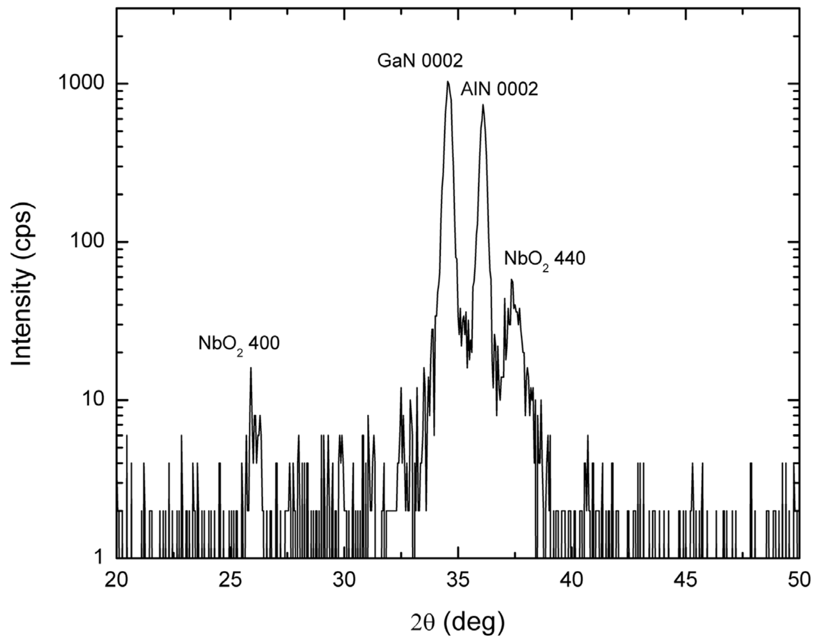

Fig. 3. Out of plane x-ray diffraction scan of NbO_2 film grown on GaN. The film is predominantly [110]-oriented with a very small amount of [100] orientation. A rocking curve scan taken about the film 440 peak shows a full width at half maximum of 0.66°.

grazing incidence in-plane $2\theta_\chi - \phi$ scans aligned along GaN $[10\bar{1}0]$ and along GaN $[\bar{2}0]$, respectively. The scans are obtained with a fixed ω and 2θ of 0.3°. For the scan where the GaN $11\bar{2}0$ *d*-spacing is observed (Fig. 5a), we see film peaks at 34.9° (d = 2.56 Å) and 37.0° (d = 2.43 Å). These spacings correspond to NbO_2 222 and 440 reflections. The reason for the two different film spacings is because of the presence of three symmetry-related domains, two of which are equivalent positive and negative 60° rotations from the other one. In addition to the main film peaks, the corresponding higher order peaks (444 and 880) as well as a weak feature at ~53.5° that may be related to a 100-oriented crystallite are also visible in the XRD scan. For the scan where the GaN $11\bar{2}0$ *d*-spacing is observed (Fig. 5b), film peaks at 62.2° (d = 1.49 Å) and 65.3° (1.43 Å) are observed. These spacings correspond to NbO_2 004 and 662 reflections. For the same reason described above, two different film in-plane spacings are observed because of the presence of three rotational domains, two of which are identical. Fig. 5 shows the epitaxial relationship between NbO_2 and GaN that is consistent with the observations in RHEED and XRD. The NbO_2 440 plane matches the GaN 0001 surface in three possible orientations leading to the pseudo-Six-fold symmetry observed.

In order to get a more complete picture of the physical structure of the film and interface, cross-section TEM was performed using both standard high resolution lattice imaging, as well as atomically resolved aberration-corrected STEM imaging. Fig. 6(a) shows a high resolution TEM image of the NbO_2 grown on GaN. The bottom shows the single crystal GaN layer with a rough top surface. In the middle is a micro-crystalline layer that is about 10 nm thick with an amorphous interfacial layer with the substrate about 1–2 nm thick. On the top is the crystalline NbO_2 layer (~12 nm). There is clearly a chemical reaction occurring between the NbO_2 and GaN producing the thick micro-crystalline layer and a thinner amorphous interfacial layer as well as a very rough GaN surface. The nature of this reaction layer is discussed in the next section.

Fig. 6(b–d) shows Fourier transforms taken of different regions of the image. Fig. 6(b) shows the Fourier transform for the top NbO_2 layer only demonstrating the crystalline nature of this layer. Fig. 6(c) is the Fourier transform for the entire image. Polycrystalline rings from the reaction layer can be seen superimposed on the diffraction spots from both the top layer and the substrate. Fig. 6(d) is the Fourier transform for the GaN layer only showing significantly sharper reflections. Typical NbO_2 domain sizes found for the sample was in the range of 15–30 nm. Fig. 7(a) shows a high-resolution HAADF image of the NbO_2 layer. This image was filtered using the yellow and blue set of reflections shown in Fig. 7(b). The image confirms the 110-orientation of the NbO_2 epitaxial layer. A zigzag pattern on the left side of the image indicates slightly misoriented grains.

3.3. Reaction layer

The reaction layer consists of two regions: a thin (<2 nm) amorphous region and a thick (~10 nm) random polycrystalline region with very small grains. Based on x-ray reflectivity measurements, the polycrystalline region appears to be nearly indistinguishable chemically from the crystalline NbO_2 top layer (nearly identical electron density) and is likely also composed of NbO_x that is highly disordered. To obtain a better understanding of the interface, electron energy loss spectroscopy (EELS) elemental maps are obtained from the STEM image of the polycrystalline region, the amorphous reaction region, and the upper surface of the GaN substrate. Fig. 8 shows elemental maps for Ga, N, Nb, and O obtained from the interface region of the sample. Oranges/yellows indicate large amounts of the element, while greens indicate moderate amounts, and blues/blacks indicate low or insignificant amounts. The upper part of the elemental maps corresponds to the polycrystalline region. This portion consists of Nb and O only with possible residual amounts of Ga. This is consistent with x-ray reflectivity measurements which do not see an electron density difference between the epitaxial layer and the polycrystalline NbO_2 top layer. The thin middle transition layer indicated by the white horizontal lines in the elemental maps corresponds to the amorphous reaction layer. The layer consists of significant amounts of O, Nb, and Ga plus minor amounts of N. The substrate subsurface as expected consists mainly of Ga and N although some Nb and O appear to have partially diffused into the subsurface region. In order to further elucidate the nature of the amorphous reaction layer, in situ XPS was performed on a sample with nominally 4 nm of NbO_2 to enable a measurement of the interface chemical composition. For a sample grown using the standard method described in Section 2 where the substrate is heated, then exposed to oxygen gas, and then followed by Nb metal deposition, the interface

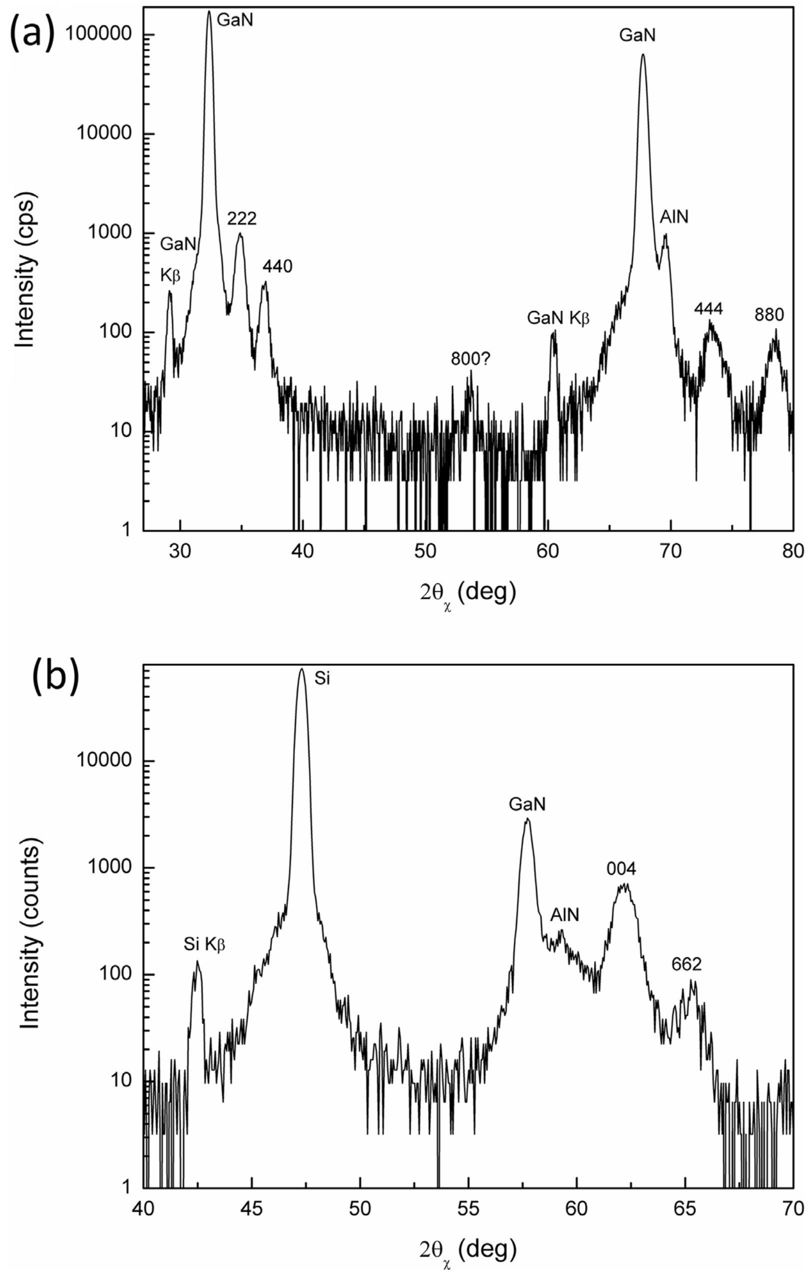

Fig. 4. Grazing incidence in-plane x-ray diffraction. Two scans centered on different high symmetry in-plane directions of GaN are shown. (a) Scan showing GaN 10-10 spacing. Film peaks from the 222 and 440 reflections are observed. (b) Scan showing GaN 11-20 spacing. Film peaks from the 004 and 662 reflections are observed.

consists of a combination of NbN, NbO_x, and GaO_x. Fig. 9(a) shows the Nb 3d core level for such a sample showing clearly the presence of NbN in addition to oxides of Nb. It is clear from Figs. 8 and 9(a) that there is a reacted region where all four elements (Ga, N, Nb, O) become intermixed. We speculate on the possible compounds present in the reaction layer by looking at the possible reactions between GaN and NbO_2 in the presence of excess O_2 (8×10^{-4} Pa). We discard the possibility of forming Nb_2O_5 as based on our and others' experience, the prevailing oxygen gas pressure is not sufficient to form Nb_2O_5 from elemental Nb [30,33]. We consider the product compounds that can form to be $NbGaO_4$, NbN, NbON, NO_x ($x = 0.5$ to 2), N_2 and Ga_2O_3. From reported values (experimental where available and calculated otherwise) of formation energies [34], we infer that the most likely reaction scenarios are the following because they have the highest (most negative) reaction enthalpies.

$$GaN + NbO_2 + 2O_2 \rightarrow GaNbO_4 + NO_2\uparrow \ (\Delta H = -853 \text{ kJ/mol})$$

$$GaN + 3/2NbO_2 + 5/4O_2 \rightarrow GaNbO_4 + 1/2NbON + 1/2NO_2\uparrow \ (\Delta H = -600 \text{ kJ/mol})$$

The amorphous layer is expected to consist mainly of $GaNbO_4$ with minor amounts of NbON. This composition would be consistent with what is observed from the STEM-EELS elemental maps and from XPS of thin layers.

It is clear that the crystalline NbO_2 layer formed is not in close contact with the substrate for samples grown using the conditions described above, making coupling between the metal-insulator transition behavior of the NbO_2 and the GaN extremely weak. This strong reactivity between NbO_2 and GaN points to the need to develop a different layer-by-layer approach, where each grown layer must be thermodynamically stable in contact with the layer above and beneath it, similar to the case for $SrTiO_3$ on Si [35]. As an initial attempt to avoid

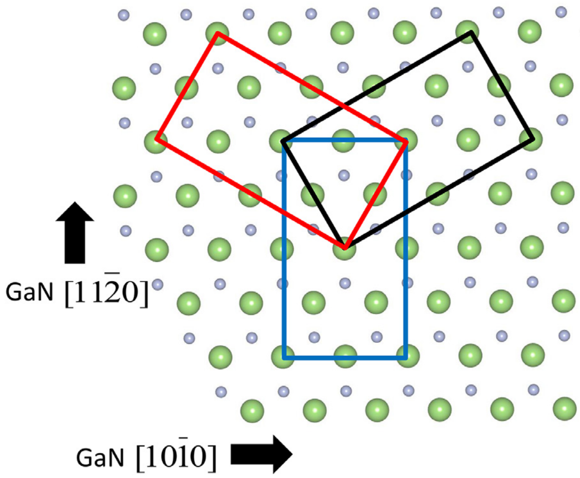

Fig. 5. Schematic diagram of the epitaxial relationship between NbO_2 and GaN. The GaN (0001) surface atomic structure is shown with surface Ga atoms in light green and subsurface N atoms in light blue. Three [110]-oriented NbO_2 surface unit cells are drawn showing the three possible alignments with the GaN surface. The three possible alignments result in pseudo-six-fold symmetry for the NbO_2 film. (For interpretation of the references to colour in this figure legend, the reader is referred to the web version of this article.)

the reaction layer, we deposit four monolayers of Ga metal on the GaN surface prior to the oxygen exposure. This forms a Ga suboxide on oxygen exposure. Depositing Nb metal in oxygen on this Ga suboxide surface appears to prevent the nitridation of Nb and NbO_2 forms directly on this surface without structural disruption as observed in RHEED (the NbO_2 film streaks emerge immediately). Fig. 9(b) shows the Nb 3d core level for a 4 nm NbO_2 film with the Ga metal insert and confirms no NbN is formed. This observation points to the possible need for inserting a buffer layer such as a Zintl phase transition layer [36] to allow for a smooth chemical environment change from GaN to NbO_2 in order to avoid the nitridation of Nb. Growing at a much higher rate may also inhibit the reaction as once NbO_2 is formed as a phase, it is stable against reaction with GaN. However, sufficiently high rates may not be accessible in standard oxide MBE deposition systems. Further studies on the growth process are clearly needed to fully utilize the metal-insulator transition in NbO_2 in GaN-based hyper-FETs.

4. Conclusions

We have grown highly textured crystalline films of NbO_2 (110) on GaN(0001)/Si(111) substrates. The films have single out of plane orientation but have three in-plane rotational domains with typical size ranging from 15 to 30 nm. We also observe a strong reaction between the incoming Nb and O_2 flux and GaN, resulting in a thin amorphous reaction layer consisting of Ga, Nb, O and N. The reaction also causes randomization of the bottom half of the NbO_2 film forming a microcrystalline NbO_x layer. A deliberate layer-sequenced approach to growing NbO_2 on GaN is needed, such as insertion of a Ga metal layer, if one wishes to avoid an interfacial chemical reaction and be able to couple the NbO_2 film with the GaN substrate.

Acknowledgments

The work in Austin is supported by the National Science Foundation under grant DMR-1507970 and by the Air Force Office of Scientific Research under Grant FA9550-18-1-0053. The authors gratefully acknowledge use of facilities and instrumentation supported by NSF through University of Wisconsin Materials Research Science and Engineering Center (DMR-1720415).

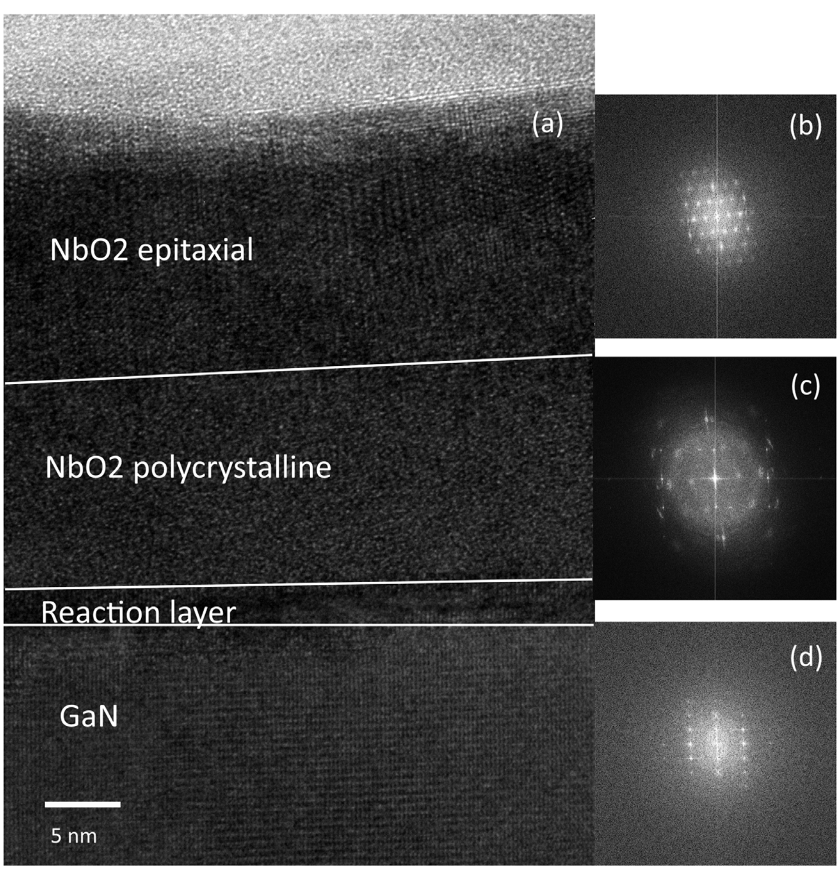

Fig. 6. High-resolution TEM image of the layer structure of NbO_2 grown on GaN. (a) A crystalline NbO_2 layer is visible as the topmost layer on top of the GaN substrate at the bottom. In between is a polycrystalline NbO_2 layer with very tiny grains. Between the polycrystalline layer and the substrate is an amorphous reaction layer. (b) Fourier transform of the crystalline NbO_2 layer. (c) Fourier transform of the entire image showing the polycrystalline arcs from the middle region. (d) Fourier transform of the GaN substrate region.

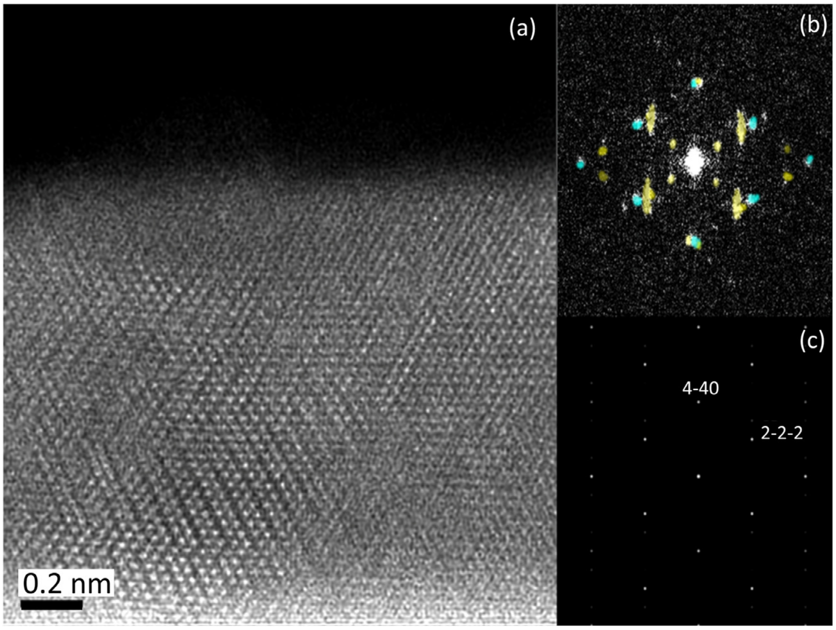

Fig. 7. Atomically resolved STEM-HAADF filtered image of NbO_2 layer. (a) STEM image of NbO_2 layer showing predominantly 110-oriented grains. A zigzag pattern corresponding to tilted grains is visible on the left side of the image. (b) Fourier transform of the entire image. Reflections marked in blue represent the [110] zone axis of NbO_2. Reflections marked in yellow show grains with a slightly different tilt but, on average, align with [110]. (c) Simulated selected area diffraction pattern for the [110] zone axis of NbO_2, matching the blue-marked reflections well.

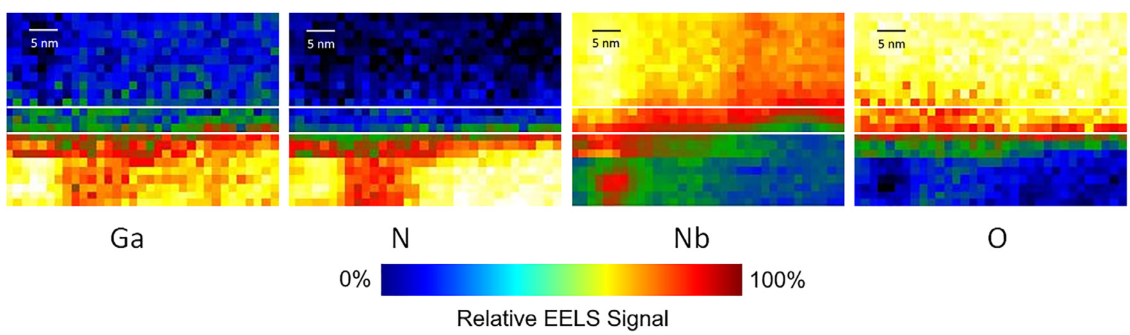

Fig. 8. EELS elemental maps of the reaction layer and the substrate. Oranges and yellows indicate high intensity, green indicates medium intensity, and blues and blacks indicate low intensity. The top layer is the polycrystalline portion of the reaction layer. The thin middle layer between the two horizontal white lines is the amorphous reaction layer. The bottom layer is the upper region of the substrate. The polycrystalline portion of the reaction layer is confirmed to be NbO_x while the amorphous reaction consists of Nb, O, Ga, and some N. There is also evidence of Nb penetration the near surface regions of the substrate. (For interpretation of the references to colour in this figure legend, the reader is referred to the web version of this article.)

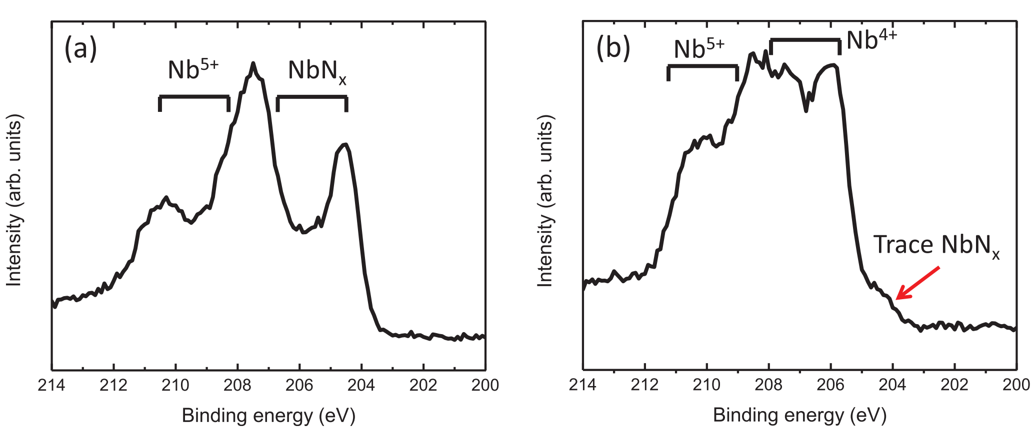

Fig. 9. Nb 3d spectra of the interface region of NbO_2 grown on GaN. (a) Nb 3d spectrum for interface grown using standard deposition process where GaN surface is exposed simultaneously to oxygen gas and Nb metal at high temperature. A significant amount of NbN_x and Nb^{5+} is observed. (b) Nb 3d spectrum for interface grown with the insertion of four monolayers of Ga metal prior to Nb deposition in oxygen. Nb^{4+} is clearly observable and only a small amount of NbN_x is formed, but Nb^{5+} oxidation state from $NbGaO_x$ is still observable.

References

[1] A.A. Demkov, A.B. Posadas, Integration of Functional Oxides with Semiconductors, Springer, New York, 2014.
[2] D.G. Schlom, L.-Q. Chen, X. Pan, A. Schmehl, M.A. Zurbuchen, A thin film approach to engineering functionality into oxides, J. Am. Ceram. Soc. 91 (2008) 2429.
[3] J.W. Reiner, A.M. Kolpak, Y. Segal, K.F. Garrity, S. Ismail-Beigi, C.H. Ahn, F.J. Walker, Crystalline oxides on silicon, Adv. Mater. 22 (2010) 2919.
[4] M. Imada, A. Fujimori, Y. Tokura, Metal-insulator transitions, Rev. Mod. Phys. 70 (1998) 1039.
[5] Z. Yang, C. Ko, S. Ramanathan, Oxide electronics utilizing ultrafast metal-insulator transitions, Annu. Rev. Mater. Res. 41 (2011) 337.
[6] S. Middey, J. Chakhalian, P. Mahadevan, J.W. Freeland, A.J. Millis, D.D. Sarma, Physics of ultrathin films and heterostructures of rare-earth nickelates, Annu. Rev. Mater. Res. 46 (2016) 305.
[7] R.F. Janninck, D.H. Whitmore, Electrical conductivity and thermoelectric power of niobium dioxide, J. Phys. Chem. Solids 27 (1966) 1183.

[8] J.C. Zolper, A review of junction field effect transistors for high-temperature and high-power electronics, Solid-State Electron. 42 (1998) 2153.
[9] M.S. Shur, GaN based transistors for high power applications, Solid-State Electron. 42 (1998) 2131.
[10] S. Nakamura, T. Mukai, M. Senoh, High-power GaN P-N junction blue-light-emitting diodes, Jpn. J. Appl. Phys. 30 (1991) L1998.
[11] S.P. Denbaars, Gallium-nitride-based materials for blue to ultraviolet optoelectronics devices, Proc. IEEE 85 (1997) 1740.
[12] S. Strite, H. Morkoc, GaN, AlN, and InN: a review, J. Vac. Sci. Technol. B 10 (1992) 1237.
[13] J.W. Orton, C.T. Foxon, Group III nitride semiconductors for short wavelength light-emitting devices, Rep. Progr. Phys. 61 (1998) 1.
[14] R.F. Davis, Z. Sitar, B.E. Williams, H.S. Kong, H.J. Kim, J.W. Palmour, J.A. Edmond, J. Ryu, J.T. Glass, C.H. Carter Jr, Critical evaluation of the status of the areas for future research regarding the wide band gap semiconductors diamond, gallium nitride and silicon carbide, Mater. Sci. Eng. B 1 (1988) 77.
[15] N. Shukla, A.V. Thathachary, A. Agrawal, H. Paik, A. Aziz, D.G. Schlom, S.K. Gupta, R. Engel-Herbert, S. Datta, A steep-slope transistor based on abrupt electronic phase transition, Nat. Commun. 6 (2015) 7812.
[16] W.Y. Tsai, X. Li, M. Jerry, B. Xie, N. Shukla, H. Liu, N. Chandramoorthy, M. Cotter, A. Raychowdhury, D.M. Chiarulli, S.P. Levitan, S. Datta, J. Sampson, N. Ranganathan, V. Narayanan, 'Enabling new computation paradigms with HyperFET—an emerging device, IEEE Trans. Multi-Scale Comput. Syst. 2 (2016) 30.
[17] C.M. Lueng, H.L.W. Chan, C. Surya, C.L. Choy, Piezoelectric coefficient of aluminum nitride and gallium nitride, J. Appl. Phys. 88 (2000) 5360.
[18] A. O'Hara, T.N. Nunley, A.B. Posadas, S. Zollner, A.A. Demkov, Electronic and optical properties of NbO2, J. Appl. Phys. 116 (2014) 213705.
[19] C.-R. Cho, J.-Y. Hwang, J.-P. Kim, S.-Y. Jeong, S.-G. Yoon, W.-J. Lee, Growth and characterization of (Ba0.5Sr0.5)TiO3 films epitaxially grown on (002) GaN/(0006) Al2O3 electrode, Jpn. J. Appl. Phys. 43 (2004) L1425.
[20] M.D. Losego, L.Fitting Kourkoutis, S. Mita, H.S. Craft, D.A. Muller, R. Collazo, Z. Sitar, J.-P. Maria, Epitaxial Ba0.5Sr0.5TiO3-GaN heterostructures with abrupt interfaces, J. Cryst. Growth 311 (2009) 1106.
[21] A. Posadas, J.-B. Yau, C.H. Ahn, J. Han, S. Gariglio, K. Johnston, K.M. Rabe, J.B. Neaton, Epitaxial growth of multiferroic YMnO3 on GaN, Appl. Phys. Lett. 87 (2005) 171915.
[22] Y. Chye, T. Liu, D. Li, K. Lee, D. Lederman, T.H. Myers, Molecular beam epitaxy of YMnO3 on c-plane GaN, Appl. Phys. Lett. 88 (2006) 132903.
[23] P.J. Hansen, Y. Terao, Y. Wu, R.A. York, U.K. Mishra, J.S. Speck, LiNbO3 thin film growth on (0001)-GaN, J. Vac. Sci. Technol. B 23 (2005) 162.
[24] L. Hao, J. Zhu, Y. Liu, S. Wang, H. Zeng, X. Liao, Y. Liu, H. Lei, Y. Zhang, W. Zhang, Y. Li, Integration and electrical properties of epitaxial LiNbO3 ferroelectric film on n-type GaN semiconductor, Thin Solid Films 520 (2012) 3035.
[25] E.A. Paisley, M.D. Losego, B.E. Gaddy, J.S. Tweedie, R. Collazo, Z. Sitar, D.L. Irving, J.-P. Maria, Surfactant-enabled epitaxy through control of growth mode with chemical boundary conditions, Nat. Commun. 2 (2011) 461.
[26] H.S. Craft, J.F. Ihlefeld, M.D. Losego, R. Collazo, Z. Sitar, J.-P. Maria, MgO epitaxy on GaN (0002) surfaces by molecular beam epitaxy, Appl. Phys. Lett. 88 (2006) 212906.
[27] P.J. Hansen, V. Vaithyanathan, Y. Wu, T. Mates, S. Heikman, U.K. Mishra, R.A. York, D.G. Schlom, J.S. Speck, Rutile films grown by molecular beam epitaxy on GaN and AlGaN, J. Vac. Sci. Technol. B 23 (2005) 499.
[28] T. Hitosugi, Y. Hirose, J. Kasai, Y. Furubayashi, M. Ohtani, K. Nakajima, T. Chikyow, T. Shimada, T. Hasegawa, Heteroepitaxial growth of rutile TiO2 on GaN(0001) by pulsed laser deposition, Jpn. J. Appl. Phys. 44 (2005) L1503.
[29] W. Tian, V. Vaithyanathan, D.G. Schlom, Q. Zhan, S.Y. Yang, Y.H. Chu, R. Ramesh, Epitaxial integration of (0001) BiFeO3 with (0001) GaN, Appl. Phys. Lett. 90 (2007) 172908.
[30] A.B. Posadas, A. O'Hara, S. Rangan, R.A. Bartynski, A.A. Demkov, Band gap of epitaxial in-plane-dimerized single-phase NbO2 films, Appl. Phys. Lett. 104 (2014) 092901.
[31] T. Hadamek, A.B. Posadas, A. Dhamdhere, D.J. Smith, A.A. Demkov, Spectral identification scheme for epitaxially grown single-phase niobium dioxide, J. Appl. Phys. 119 (2016) 095308.
[32] C.D. Wagner, L.E. Davis, M.V. Zeller, J.A. Taylor, R.M. Raymond, L.H. Gale, Empirical atomic sensitivity factors for quantitative analysis by electron spectroscopy for chemical analysis, Surf. Interface Anal 3 (1981) 211.
[33] M. Petrucci, C.W. Pitt, S.R. Reynolds, H.J. Milledge, M.J. Mendelssohn, C. Dineen, W.G. Freeman, Growth of thin-film niobium and niobium oxide layers by molecular-beam epitaxy, J. Appl. Phys. 63 (1988) 900.
[34] A. Jain, S.P. Ong, G. Hautier, W. Chen, W.D. Richards, S. Dacek, S. Cholia, D. Gunter, D. Skinner, G. Ceder, K.A. Persson, Commentary: the materials project: a materials genome approach to accelerating materials innovation, APL Mater. 1 (2013) 011002.
[35] A.M. Kolpak, S. Ismail-Beigi, Thermodynamic stability and growth kinetics of epitaxial SrTiO3 on silicon, Phys. Rev. B 83 (2011) 165318.
[36] A.A. Demkov, H. Seo, X. Zhang, J. Ramdani, Using Zintl-Klemm intermetallics in oxide-semiconductor heteroepitaxy, Appl. Phys. Lett. 100 (2012) 071602.